Supporting Information

Pyridylamine Templated Borate-Derived Co nanoparticles Anchored on N-Doped Carbon for Enhanced Oxygen Reduction Reaction in Al-Air Batteries

*Xiao-Ting Zhang, Cun-Mao Chen, Qi-Ming Huang and Chun-Yang Pan**

School of Light Industry and Chemical Engineering, Guangdong University of Technology, Guangzhou, Guangdong 510006, China

**Corresponding author*
E-mail: panchuny@gdut.edu.cn

1. Materials

The $Co(CH_3COOH)_2$, H_3BO_3, 20 wt% Pt/C and KOH were obtained from Shanghai Macklin Co., Ltd. DPA(2,2'-dipicolylamine) and 2-AMP(2-(aminomethyl)pyridine) were purchased from Shanghai BiDe Pharmaceutical Technology Co., Ltd. RuO_2 was purchased from Shanghai Aladdin Biochemical Technology Co., Ltd. Pyridine was obtained from Tianjin Damao Co., Ltd. Nafion solution (5 wt%) and PTFE(D-210C) were obtained from Sinero. All reagents were used without any further treatment before use.

2. Characterization

Transmission electron microscopy (TEM) analysis was conducted using a FEI Talos F200X G2 instrument. Energy-Dispersive X-ray Spectroscopy (EDS): Super-X EDS system with four silicon-drift detectors (SDDs), enabling high-sensitivity elemental mapping and quantitative compositional analysis at nanoscale resolution. Fourier-transform infrared (FTIR) spectra were collected on a Thermo Fisher Scientific iS50R spectrometer. Powder X-ray diffraction (PXRD) patterns were recorded on a Bruker D8 Advance X-ray diffractometer. The Brunauer-Emmett-Teller (BET) method was employed to determine the specific surface area, while the Barrett-Joyner-Halenda (BJH) model was used to calculate the pore size distribution of the samples. X-ray photoelectron spectroscopy (XPS) analysis was performed on a Thermo Scientific Nexsa instrument equipped with an Al Kα excitation source (1486.7 eV) for surface chemical analysis. Raman spectra were collected using a Horiba LabRAM HR Evolution spectrometer.

3. Single Crystal X-ray Diffraction

Single Crystal X-ray diffraction data were collected using a Bruker D8 Quest diffractometer (Mo Kα, λ= 0.71073 Å). Indexing and data integration were performed using APEX3 (Difference Vectors method). Absorption correction was performed by multiscan method implemented in SADABS. Space groups were determined using XPREP implemented in APEX3. Structures were solved using SHELXL-2014 (direct methods) and refined using SHELXL-2014 (full-matrix least-squares on F2) with anisotropic displacement contained in

APEX3 program packages. Hydrogen atoms on carbon and nitrogen were calculated in ideal positions with isotropic placement parameters set to 1.2 × U_{eq} of the attached atoms.

4. Electrochemical Measurements.

A standard three-electrode system electrochemical workstation (CHI660E) was used to evaluate the electrocatalytic performance of the prepared catalyst. 5 mg of catalyst powder was dispersed in 1 ml of ethanol and 20 μl of nafion solution (5 wt%), and then ultrasonicated for 30 minutes to obtain the catalyst ink. Then, 5 μl of the catalyst ink was dropped onto the surface of the working electrode, and the ink was dried to form a film on the surface and then the above operation was repeated four times. A graphite rod was used as the counter electrode, and a Hg/HgO electrode served as the reference electrode. All recorded potentials were calibrated to the reversible hydrogen electrode (RHE) using the equation:

$$E_{RHE} = E_{Hg/HgO} + 0.0592 \times pH + 0.098.$$

Cyclic voltammetry (CV) measurements were performed at a scan rate of 50 mV s^{-1} in an O_2-saturated 0.1 M KOH solution. Linear sweep voltammetry (LSV) was conducted on a rotating disk electrode (RDE) at 1600 rpm with a scan rate of 5 mV s^{-1}. The electrochemical double-layer capacitance (Cdl) was extracted from CV curves in the non-Faradaic potential range (0.9176 to 1.0176 V vs. RHE) to estimate the electrochemically active surface area (ECSA) of the electrocatalyst.

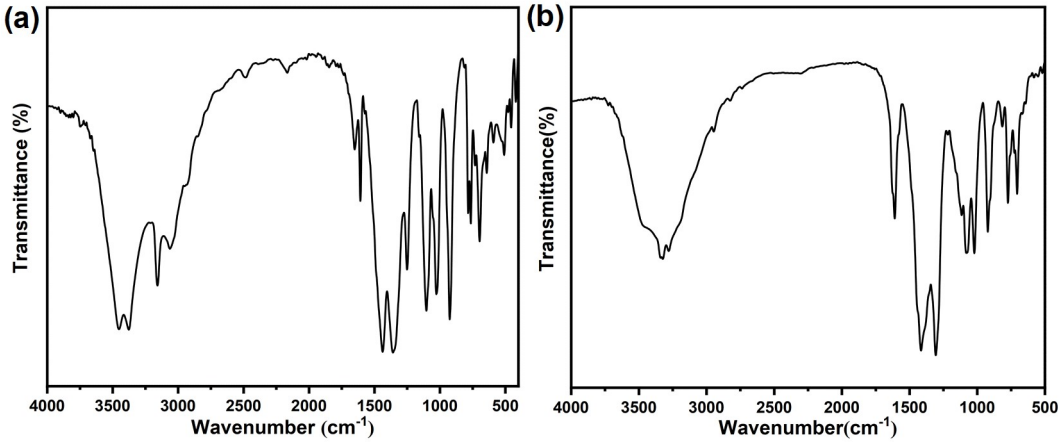

Fig. S1. (a) The FTIR spectra of **1**. (b) The FTIR spectra of **2**.

The FTIR spectra of **1** and **2** are shown in **Fig. S1**. The broad absorption bands at 3455-3378 cm^{-1} (**1**) and 3342-3280 cm^{-1} (**2**) are attributed to the asymmetric stretching vibration of O-H bonds. Characteristic peaks in the 3158-2815 cm^{-1} range likely originate from symmetrical stretching vibrations of C-H and N-H groups. Distinct absorption features appearing at 1436-1365 cm^{-1} (**1**) and 1411-1307 cm^{-1} (**2**) are associated with B-O asymmetric stretching vibrations in BO_3 groups. Meanwhile, the B-O asymmetric stretching vibrations of BO_4 groups are detected at 1103-923 cm^{-1} (**1**) and 1078-923 cm^{-1} (**2**).

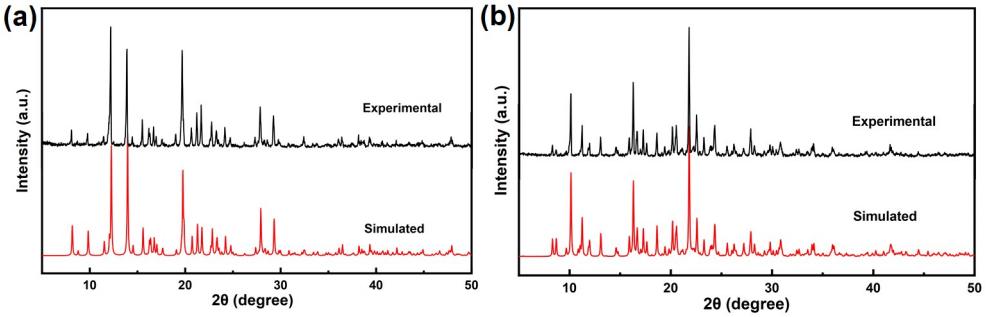

Fig. S2. (a)The PXRD patterns of **1**. (b)The PXRD patterns of **2**.

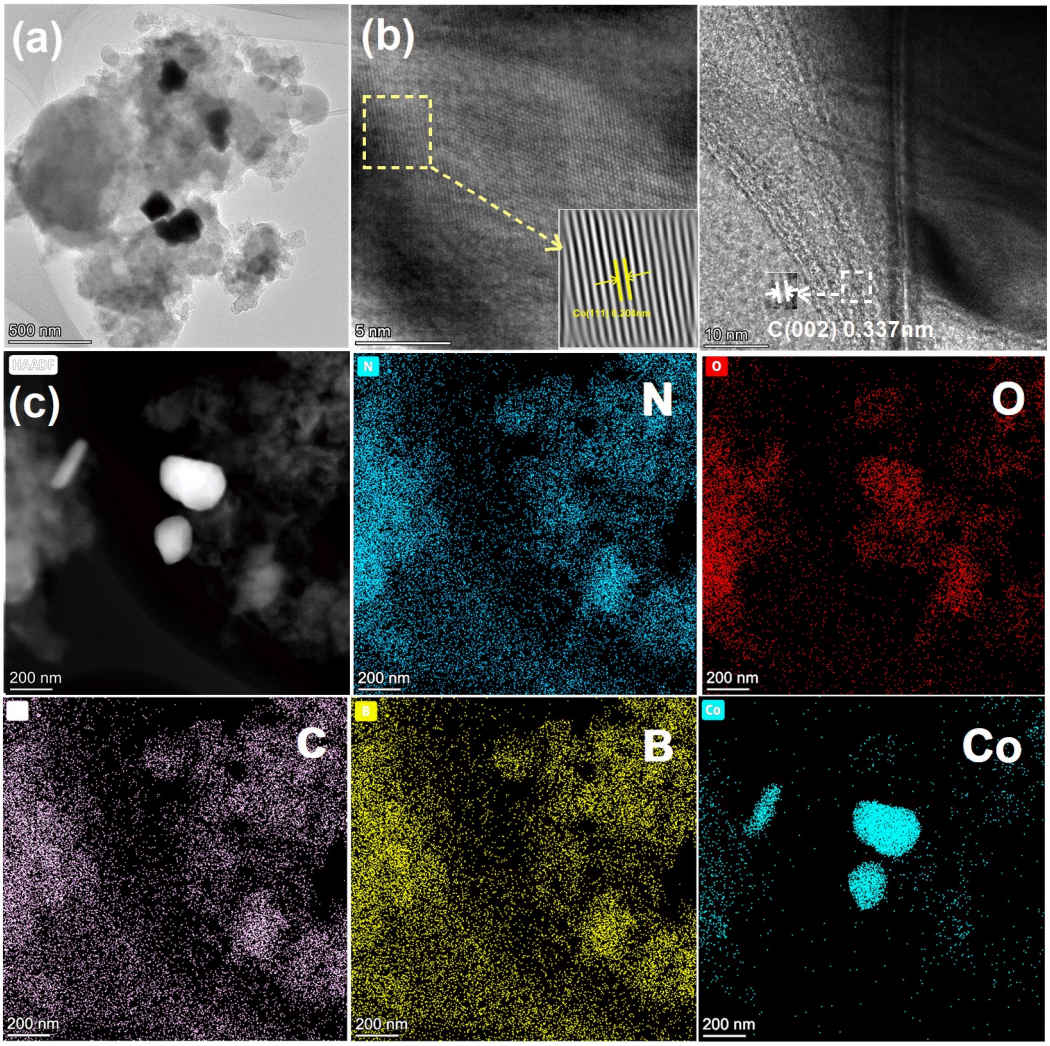

Fig. S3. (a) TEM images of Co2/600. (b) HRTEM images of Co2/600. (c) HAADF-STEM and EDS element mapping of Co2/600.

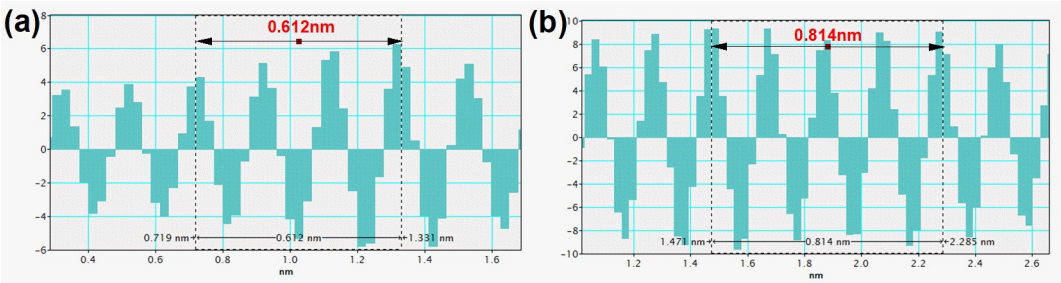

Fig. S4. (a) Lattice spacing measurement of Co1/750. (b) Lattice spacing measurement of Co2/600.

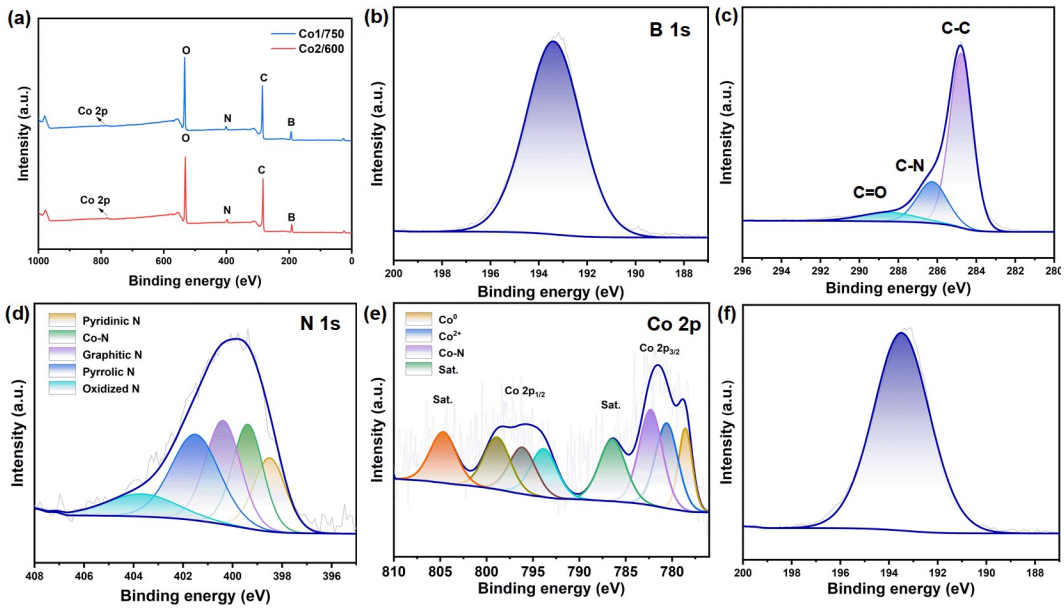

Fig. S5. XPS patterns. (a) Co1/750 and Co2/600 survey; (b) B 1s for Co1/750; (c) C 1s for Co2/600; (d) N1s for Co2/600; (e) Co2p for Co2/600; (f) B 1s for Co2/600;

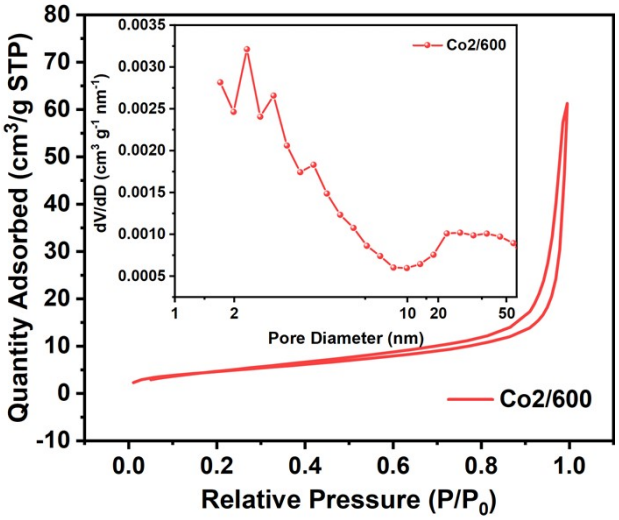

Fig. S6. N_2 adsorption–desorption isotherms of Co2/600 (Inset is the pore size distribution of Co2/600)

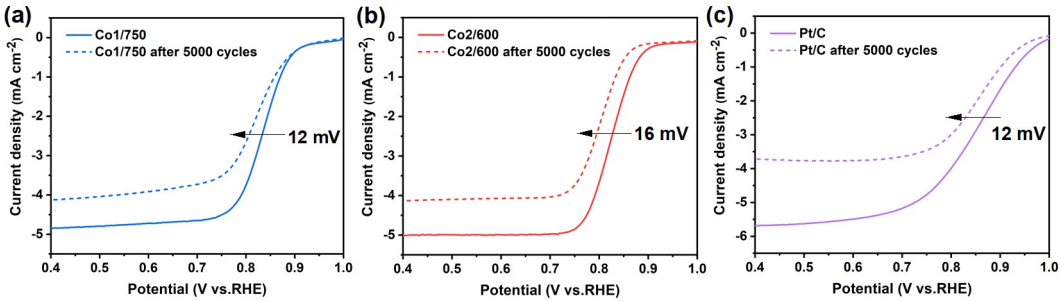

Fig. S7. (a),(b) and (c) LSV curves before and after 5000 CV cycles of Co1/750, Co2/600 and Pt/C.

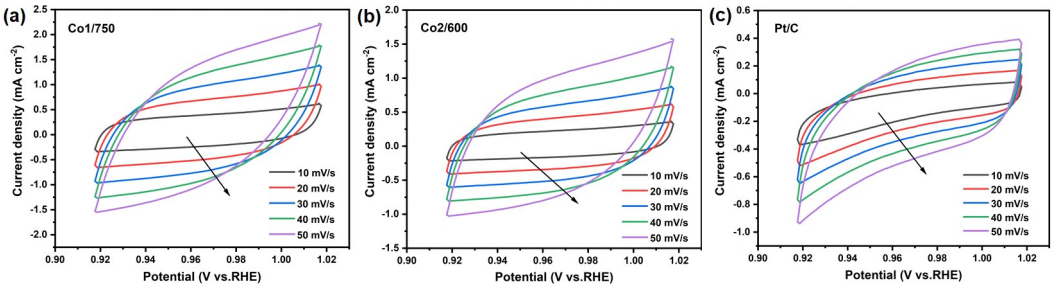

Fig. S8. (a) CV curves of Co1/750. (b) Co2/600 and (c) Pt/C in O_2-saturated 0.1 M KOH solution at scan rates from 10 to 50 mV s^{-1}.

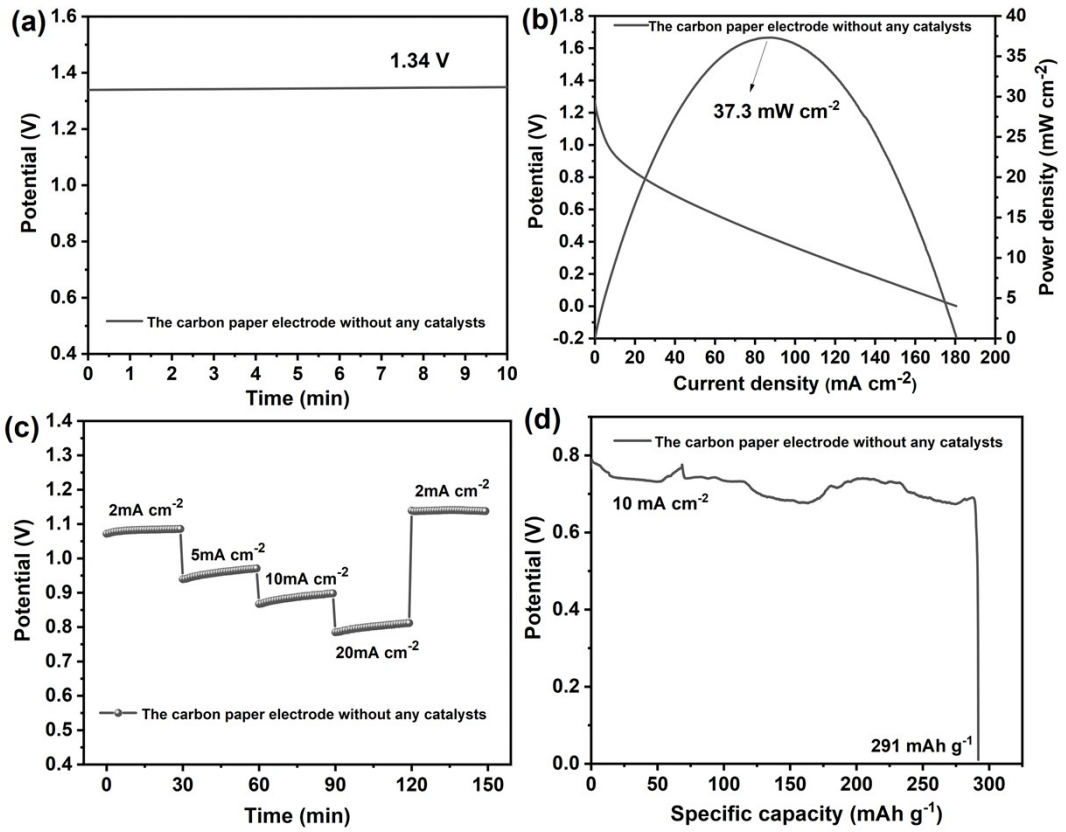

Fig. S9. Electrochemical performance of Al-air batteries with a bare carbon paper cathode. (a) Open-circuit voltages. (b) Discharge polarization curves and power density curves. (c) Discharge curves of the carbon paper electrode without any catalysts. (d) Specific capacity of the Al-air battery for the carbon paper electrode without any catalysts.

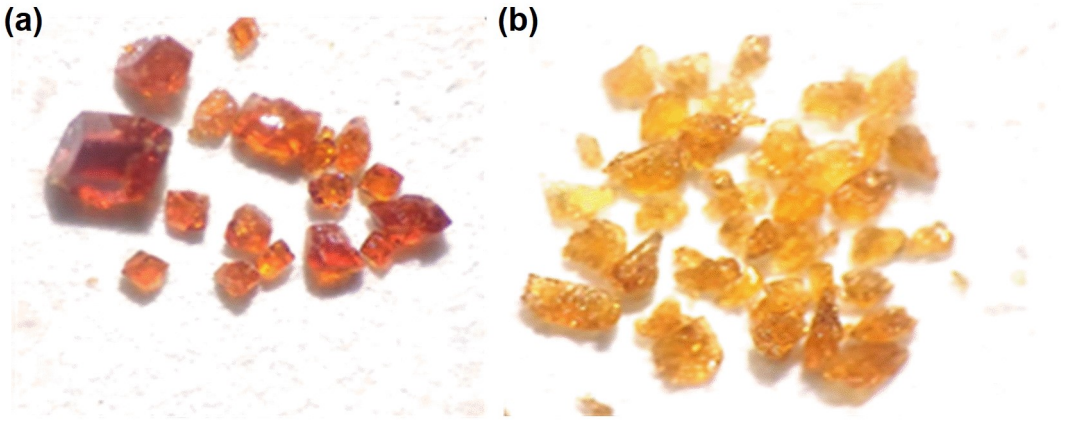

Fig. S10. Crystals. (a) **1**; (b) **2**.

Table S1. Crystal data and structure refinement for **1** and **2**

compound	**1**	**2**
Empirical formula	$[Co(DPA)_2][B_{10}O_{13}(OH)_6]$	$[Co(2\text{-}AMP)_3][B_5O_6(OH)_4]_2$
Formula weight	875.58	819.52
Temperature/K	150.15	150.15
Crystal system	monoclinic	triclinic
Space group	*C*2/c	*P*-1
a/Å	23.1566(16)	9.4975(9)
b/Å	11.3635(7)	11.2097(11)
c/Å	15.4461(9)	17.3553(18)
α/°	90	73.016(3)
β/°	110.943(2)	76.158(3)
γ/°	90	78.491(3)
Volume/Å^3	3796.0(4)	1699.0(3)
Z	4	2
ρ_{calc}g/cm^3	1.532	1.602
μ/mm^{-1}	0.538	0.597
F(000)	1788.0	838.0
Crystal size/mm^3	0.3 × 0.3 × 0.29	0.3 × 0.25 × 0.18
Radiation	MoKα (λ = 0.71073)	MoKα (λ = 0.71073)
2θ range for data collection/°	5.308 to 50.018	4.46 to 50.184
Index ranges	-27 ≤ h ≤ 24, -13 ≤ k ≤ 13, -18 ≤ l ≤ 18	-10 ≤ h ≤ 11, -13 ≤ k ≤ 12, -20 ≤ l ≤ 20
Reflections collected	24722	22125
Independent reflections	3350 [R_{int} = 0.0432, R_{sigma} = 0.0300]	6008 [R_{int} = 0.0886, R_{sigma} = 0.1112]
Goodness-of-fit on F^2	1.059	1.010
Final R indexes [I>=2σ (I)]	R_1 = 0.0360, wR_2 = 0.0744	R_1 = 0.0689, wR_2 = 0.1316
R indexes (all data)[a]	R_1 = 0.0538, wR_2 = 0.0836	R_1 = 0.1522, wR_2 = 0.1650

[a] $R_1 = \Sigma||Fo| - |F||/\Sigma|Fo|$ and $wR_2 = [\Sigma w (Fo^2 - Fc^2)^2 / \Sigma wFo^4]^{1/2}$

Table S2. The element content of Co1/750 and Co2/600 was obtained by XPS.

Co1/750	Element	C	N	O	Co	B
	Content	44.28 at%	3.11 at%	31.29 at%	0.29 at%	21.03 at%
Co2/600	Element	C	N	O	Co	B
	Content	44.36 at%	3.55 at%	30.78 at%	0.42 at%	20.89 at%

Table S3. Borate-Based Catalysts and Their ORR Performances in Recent Studies.

Name of catalyst	**$E_{1/2}$ [V vs. RHE]**	**Year**	**Electrolyte**	**Ref.**
$[Co_2(bpy)_4(C_2O_4)]\cdot[B_5O_6(OH)_4]_2\cdot py_2$	0.82 V	2025	0.1 M KOH	[1]
$[Cu(en)_2]\cdot[B_4O_5(OH)_4]\cdot 2H_3BO_3$	0.817 V	2024	1 M KOH	[2]
$CSF127B_1$	0.821 V	2024	0.1 M KOH	[3]
NiCoFeB	0.723 V	2023	0.1 M KOH	[4]
rGO/CB/Co−Bi	0.70 V	2018	0.1 M KOH	[5]
$[Co(DPA)_2][B_{10}O_{13}(OH)_6]$	0.84 V	-	0.1 M KOH	This work
$[Co(2\text{-}AMP)_3][B_5O_6(OH)_4]_2$	0.82 V	-	0.1 M KOH	This work

Table S4. The performance comparison of present reported Liquid Al-air battery.

Catalyst	**Open circuit potential(V)**	**Peak power density(mW cm^{-2})**	**Ref**
Co1/750	1.56	191	This work
Co2/600	1.54	178	This work
FeCo-PBA	1.68	98.62	[6]
$FeCoP_2$-NPWC	1.52	87.1	[7]
Co-N-C	-	174	[8]
CoNi@NCNTs/CC	1.682	151	[9]
Co@N/GNP	1.61	143.04	[10]

CMNC-1	1.78	139.8	[11]
MCM-450	1.61	151	[12]
Cu-Fe-CN	-	129.73	[13]
FePc-TCNB	1.64	137	[14]

References

[1] L. Liu, X.-Y. Huang, H. Liu, A.-N. Chen and C.-Y. Pan, *Chem. Eur. J.*, 2025, **31**, e202500584.

[2] A.-N. Chen, L. Liu and C.-Y. Pan, *Inorg. Chim. Acta*, 2024, **570**, 122179.

[3] Y. Yin, D. Ma, H. Liu, G. Wang, C. Lin and J. Ma, *Sustainable Energy Fuels*, 2024, **8**, 2880-2888.

[4] M. Moloudi, A. Noori, M. S. Rahmanifar, Y. Shabangoli, M. F. El-Kady, N. B. Mohamed, R. B. Kaner and M. F. Mousavi, *Adv. Energy Mater.*, 2023, **13**, 2203002.

[5] J. Q. Sun, D. J. Yang, S. Lowe, L. J. Zhang, Y. Z. Wang, S. L. Zhao, P. R. Liu, Y. Wang, Z. Y. Tang, H. J. Zhao, X. D. Yao, *Adv. Energy Mater.*, 2018, **8**, 1801495.

[6] L. Cui, M. Chen, G. Huo, X.-Z. Fu and J.-L. Luo, *Chem. Eng. J.*, 2020, **395**, 125158.

[7] W. Chen, H. Yu, S. Chang, W. Li, R. Liu, Y. Wang, H. Zhang and Z. Zhang, *Appl. Surf. Sci*., 2022, **573**, 151486.

[8] Q. Wang, X. Xu and D. Lu, *Appl. Catal. A*, 2022, **646**, 118847.

[9] W.-W. Tian, J.-T. Ren and Z.-Y. Yuan, *Appl. Catal. B Environ*, 2022, **317**, 121764.

[10] S. Jeong, S. Kim, H. Son and O. L. Li, *Catal. Today*, 2023, **420**, 114025.

[11] K. Li, R. Cheng, Q. Xue, T. Zhao, F. Wang and C. Fu, *ACS Appl. Mater. Interfaces*, 2023, **15**, 9150-9159.

[12] B. Cui, Y. Zhu, T. Hu, J. Liu, J. Wu, Y. Liu, J. Zhang, R. Shi, Z. Ba, J. Wang and J. Yang, A*ppl. Surf. Sci.*, 2025, **709**, 163823.

[13] K. Liu, K. Hu, N. Zhang, Y. Ling, X. Guan, T. Xu, A. Zhang, J. Wang, X. Liu and X. Fu, *New J. Chem.*, 2024, **48**, 12153-12161.

[14] X. Dong, J. Liu, X. Li, H. Li, X. Zhang, Y. Chen, S. Tao and J. Zhang, *ACS Appl. Mater. Interfaces*, 2025, **17**, 43135-43144.